



Directional Excitation of Surface Plasmon Polaritons by Circularly Polarized Vortex Beams

Qing Tu¹ · Jianxun Liu¹ · Shaolin Ke² · Bing Wang¹ · Peixiang Lu^{1,2}

Received: 23 July 2019 / Accepted: 3 November 2019 / Published online: 8 December 2019
© Springer Science+Business Media, LLC, part of Springer Nature 2019

Abstract

We investigate the excitation of surface plasmon polaritons (SPPs) using a metallic nanoaperture array illuminated by circularly polarized Laguerre–Gaussian (LG) vortex beams. The direction of SPP excitation is tunable by changing the circular polarization and topological charge of LG beams. The left- or right-handed circular polarization determines SPP propagation on either side of the nanoaperture array. Furthermore, varying the topological charge of LG beam will result in beam splitting of SPPs. We also utilize a composite nanoaperture array with different periods to achieve unidirectional excitation of SPPs. The study provides an interesting approach to control the excitation direction of SPPs and may find great applications in SPP generators and optical switches.

Keywords Surface plasmon polaritons · Directional excitation · Laguerre-Gaussian beam

Introduction

Surface plasmon polaritons (SPPs) are excited due to the coupling of incident light and collective oscillations of electrons at the interface of metal and dielectric, the field of which can be tightly confined and strongly enhanced on the metal surface [1, 2]. SPPs have been investigated intensively in plasmonic circuits [3], second harmonic generation [4–9], photolithography [10, 11], photodetectors [12–14], and solar cells [15, 16]. Since the wavevector of SPPs is larger than that of incident light in free space, they cannot be directly coupled to each other. Traditional approaches to excite SPPs like the Kretschmann prism [2] usually brings about bulk size of optical elements. Subwavelength scatters [17, 18] may benefit to developing compact SPP generators, but the excitation efficiency is relatively low. Metallic subwavelength grating [19–22] could be a proper candidate to reach both acceptable element size and excitation efficiency.

Exciting SPP efficiently in a well-defined direction evokes many considerations in recent years. A diversity of optical configurations such as metallic slits [23–29], ridges [30–32], and nanoantennas [33–35] have been proposed to achieve unidirectional excitation of SPPs. The metasurfaces have also been employed to improve the efficiency of SPP excitation [36, 37]. Apart from utilizing asymmetric structures and incident angles, the excitation direction is also tunable by changing the polarization of incident waves [38, 39]. Since polarized incident waves possess certain spin angular momentum (SAM), the SPP excitation can be contributed to the scheme of spin-orbit coupling [40, 41]. On the other hand, the direction of SPP excitation can also be manipulated by the orbital angular momentum (OAM) [42], which is usually yielded by using Laguerre-Gaussian (LG) vortex beam [43, 44].

In this work, we shall investigate the directional excitation of SPPs on a metallic metasurface illuminated by circularly polarized LG beams [45], which possess both SAM and OAM. The metasurface is composed of a periodic nanoaperture array on metal surface with each period of the array constructed by perpendicularly oriented nanoapertures. Since the SAM is associated with the polarization of incident beam, it could determine the side direction of SPPs propagating on the metal surface. On the other hand, the OAM related to the topological charge of the LG beam will arouse beam splitting of SPPs on both sides of the array. The excitation direction is governed by the matching condition of wavevectors concerning the incident beam and SPPs together

✉ Bing Wang
wangbing@hust.edu.cn

¹ Wuhan National Laboratory for Optoelectronics and School of Physics, Huazhong University of Science and Technology, Wuhan 430074, China

² Hubei Key Laboratory of Optical Information and Pattern Recognition, Wuhan Institute of Technology, Wuhan 430205, China

with the reciprocal lattice vector of the array. The reciprocal lattice vector of the array can compensate the difference of wavevectors between the incident beam and SPPs. By using a composite array with different periods, the beam splitting should be restrained and SPPs are excited in a single direction on the metal surface. The direction and splitting angle of SPP excitation will be discussed in detail. The study provides an efficient approach to control the excitation direction of SPPs and may find promising applications in nanoscale optical sources and switches.

Structure and Principle

The structure used to excite SPPs is shown in Fig. 1a. The LG beam with a phase factor $\exp(i\ell\varphi)$ is normally incident on the gold film with a thickness of 200 nm, where ℓ stands for the topological charge and φ is the azimuthal angle. A metallic nanoaperture array (MNA) is supposed to be fabricated on the film, which can couple LG beam to SPPs. The wavevector of SPPs is given by

$$k_{\text{SPP}} = k_0 \sqrt{\frac{\varepsilon_d \varepsilon_m}{\varepsilon_d + \varepsilon_m}}, \quad (1)$$

where $k_0 = 2\pi/\lambda$ with $\lambda = 632.8$ nm being the incident wavelength in air. ε_m denotes the relative permittivity of gold and $\varepsilon_d = 1$. The wavelength of SPPs is given by $\lambda_{\text{SPP}} = 2\pi/k_{\text{SPP}}$. The width of the MNA is $W = 5 \mu\text{m}$ and the length $L = 15 \mu\text{m}$. In each period of the array, there are two columns of nanoapertures with a distance d , which are oriented at angles 45° and 135° with respect to the x -axis, as shown in Fig. 1b. Thus, the corresponding apertures in the two columns are vertical to each other. The length and width of the nanoapertures are given by $l = 200$ nm and $w = 40$ nm, respectively. The period of the MNA is denoted by p . It should be mentioned that only the electric field components of the

incident light that are perpendicular to the apertures could efficiently excite SPPs, as depicted with \mathbf{E}_1 and \mathbf{E}_2 in Fig. 1b. For incident light with linear or circular polarization, the electric field can be decomposed into two orthogonal components \mathbf{E}_1 and \mathbf{E}_2 , as shown in the inset of Fig. 1. The phase difference between \mathbf{E}_1 and \mathbf{E}_2 is $\pm\pi$ for linear polarization incidence. For circular polarization, the phase difference should be $\pm\pi/2$. Furthermore, if the distance of two nearest apertures $d = \lambda_{\text{SPP}}/4$, the launched SPP from the left aperture will acquire an additional phase of $\pi/2$ when it propagates to the right one. When the light with left-handed circular polarization (LCP) impinges on the MNA, the excited SPPs will experience constructive interference on the left side of the array and destructive interference on the right. Consequently, SPPs will be excited and propagate on the left side of metal surface. As the light with right-handed circular polarization (RCP) is incident, the SPPs will only couple to the right. For linearly polarized light incidence, SPPs will propagate evenly on both sides of the array since linear polarization can be decomposed by LCP and RCP.

As the circularly polarized LG beam impinges on the MNA, the direction of SPP excitation can be flexibly controlled by the circular polarization and topological charge of the beam. The amplitude of the LG beam is given by [44].

$$LG_{p\ell} = \sqrt{\frac{2p!}{\pi(p+|\ell|)!} \frac{1}{w(z)} \left[\frac{\sqrt{2}r}{w(z)}\right]^{|\ell|}} \exp\left[\frac{-r^2}{w^2(z)}\right] L_p^{|\ell|}\left(\frac{2r^2}{w^2(z)}\right) \exp(i\ell\varphi) \exp\left[\frac{ik_0 r^2 z}{2(z^2+z_R^2)}\right] \exp\left[-i(2p+|\ell|+1)\tan^{-1}\left(\frac{z}{z_R}\right)\right], \quad (2)$$

where $w(z) = w_0[1 + (z/z_R)^2]^{1/2}$ is the beam radius at distance z , w_0 is the beam waist, and z_R is the Rayleigh range. The Gouy phase is given by $(2p + |\ell| + 1)\tan^{-1}(z/z_R)$. The Laguerre polynomials $L_p^{|\ell|}(x) = 1$ since the radial nodes are equal to 0 in the system. For a vortex LG beam with twisted phase distribution, the positive and negative topological charges will lead to

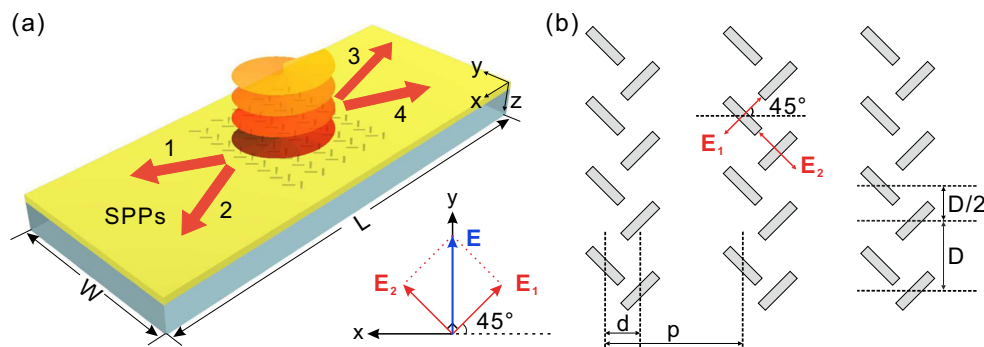


Fig. 1 **a** Schematic of the directional plasmonic coupler that is able to selectively control the emitting channels of SPPs. The red arrows indicate the four alternative paths of the SPPs excitation. **b** Specific structural details of the MNA. For the two apertures with perpendicular orientation, the horizontal distance is d and the vertical distance is $D/2$.

D and p represent the periodic space of the aperture pairs in the y - and x -coordinate directions, respectively. The field components \mathbf{E}_1 and \mathbf{E}_2 are orthogonal. The inset in the center depicts decomposition of incident electric field

contrary rotation of phase and opposite directions of the OAM in the x - y plane. The OAM of LG beam arouses in-plane wavevectors \mathbf{k}_{OAM} along azimuthal directions, as shown in Fig. 2a. $\mathbf{k}_a \sim \mathbf{k}_d$ denote the effective in-plane wavevectors that satisfy the wavevector matching conditions for $\ell = 1$. Correspondingly, $\mathbf{k}_{a'} \sim \mathbf{k}_{d'}$ are effective in-plane wavevectors for $\ell = -1$. The directions of \mathbf{k}_{OAM} are reversed for opposite topological charges. The in-plane wavevector of LG beam could be given by $k_{\text{OAM}} = \ell\pi/[2r(\ell)]$, where $r(\ell)$ is the effective radius of the LG beam with topological charge ℓ . In the cases of $\ell = \pm 1$,

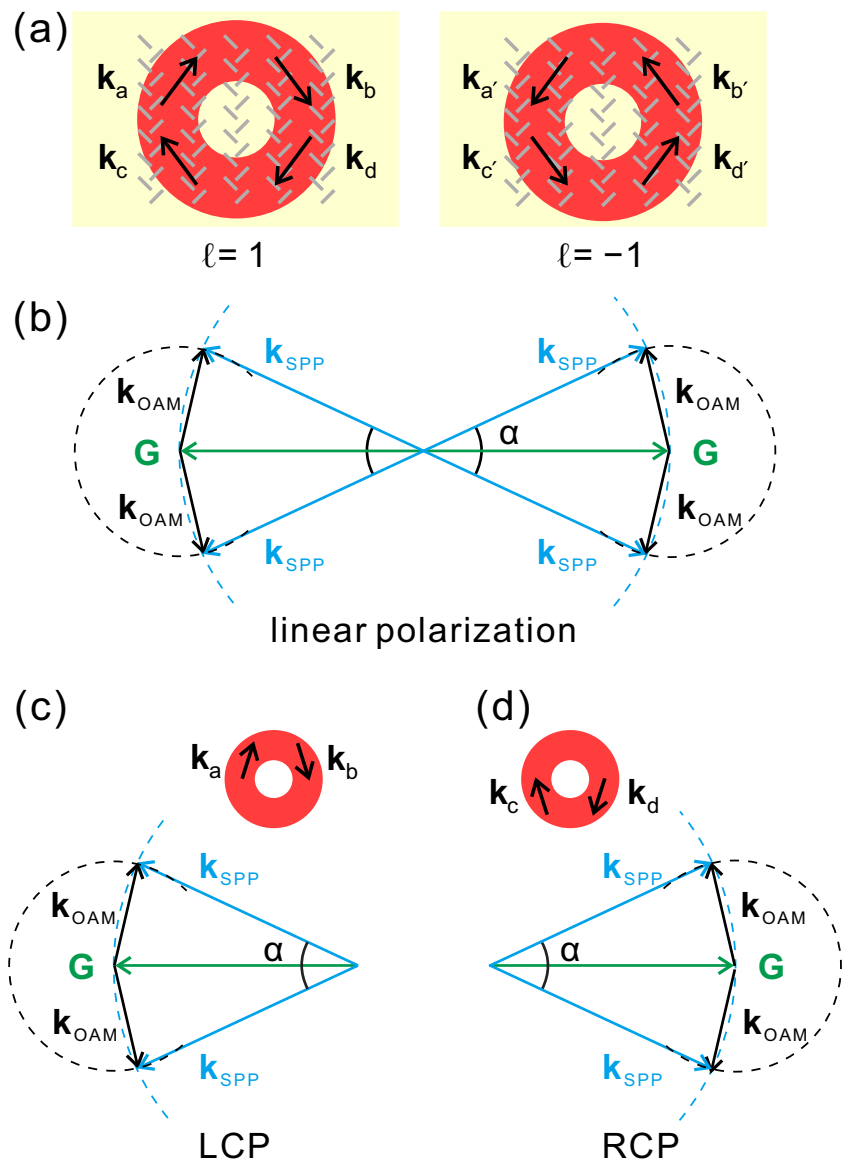
$$r(\ell) = \frac{w_0}{\sqrt{2}} \sqrt{1 + \left(\frac{z}{z_R}\right)^2}, \quad z_R = \frac{\pi w_0^2}{\lambda}. \tag{3}$$

Fig. 2 **a** Schematic of the MNA structure and in-plane wavevectors associated with OAMs of LG beams (red rings). $\mathbf{k}_a \sim \mathbf{k}_d$ and $\mathbf{k}_{a'} \sim \mathbf{k}_{d'}$ represent the in-plane wavevectors for $\ell = 1$ and $\ell = -1$, respectively. **b** Wavevector matching conditions for exciting SPPs. \mathbf{k}_{SPP} , \mathbf{G} , and \mathbf{k}_{OAM} denote the wavevectors of SPPs, reciprocal lattice vector of MNA, and in-plane wavevector of LG beam, respectively. α is the splitting angle of excited SPPs on each side of the MNA. There are four possible directions of \mathbf{k}_{OAM} that can satisfy the wavevector matching condition, corresponding to $\mathbf{k}_a \sim \mathbf{k}_d$ for $\ell = 1$ and $\mathbf{k}_{a'} \sim \mathbf{k}_{d'}$ for $\ell = -1$. **c** Wavevector matching condition for illumination of LG beam with LCP as $\ell = 1$. **d** Wavevector matching condition for illumination of LG beam with RCP as $\ell = 1$

In order to excite SPPs, the wavevector matching condition below has to be satisfied,

$$\mathbf{G} + \mathbf{k}_{\text{OAM}} = \mathbf{k}_{\text{SPP}}, \tag{4}$$

where $G \equiv |\mathbf{G}| = 2\pi/p$ is the reciprocal lattice vector of the MNA. The amplitudes of \mathbf{G} and \mathbf{k}_{SPP} are determined by the array period and Eq. (1), respectively. When fixing the incident LG beam spot size and topological charge, the amplitude of \mathbf{k}_{OAM} is also determined. Then, the directions of \mathbf{k}_{SPP} and \mathbf{k}_{OAM} can be figured out by plotting two circles with radius $|\mathbf{k}_{\text{SPP}}|$ and $|\mathbf{k}_{\text{OAM}}|$, which are centered at the start and ending points of vector \mathbf{G} , respectively. The intersection points of the two circles are the shared ending points of \mathbf{k}_{SPP} and \mathbf{k}_{OAM} , as shown in Fig. 2b. There are four solutions for Eq. (4), indicating four possible propagation directions of the excited SPP



beams for a certain topological charge such as $\ell = 1$ with linear polarization. Since the direction of SPP excitation by MNA is sensitive to the circular polarization of incident waves, the SPPs should propagate on only one side of the MNA if the LG beam is circularly polarized. Figure 2 c and d show the wavevector matching conditions and corresponding directions of \mathbf{k}_{OAM} in LCP and RCP circumstances as $\ell = 1$. For incident light with LCP, \mathbf{k}_a and \mathbf{k}_b can satisfy the wavevector matching condition, while \mathbf{k}_c and \mathbf{k}_d take effect for RCP incidence. As the topological charge becomes negative, the wavevector matching condition can still be satisfied. In this case, LG beam offers in-plane wavevectors of the same directions in different locations of beam spot that are symmetric to the former with respect to the spot center. For larger topological charge, the OAM-associated wavevector becomes larger accordingly. The higher order reciprocal lattice vector may take part in the wavevector matching. However, the SPP excitation efficiency should become lower. In this regard, we only consider the case $|\ell| = 1$ in the present work.

Results and Discussions

To validate the above analysis, we perform numerical simulations for SPP excitation and propagation by using finite-difference time-domain (FDTD) method. First, we consider a MNA structure consisting of five columns of nanoapertures. The wavelength of incidence is $\lambda = 632.8$ nm, and the corresponding SPP wavelength $\lambda_{\text{SPP}} = 603$ nm with the refractive index of gold obtained from the experimental data [46]. The period of the array $p = 600$ nm. The other parameters are given by $D = 300$ nm and $d = 150$ nm. The normally incident LG beam is aligned to the center of the MNA. The beam width of LG beam is supposed to cover more apertures to achieve higher efficiency of SPP generation.

The numerical simulation results are shown in Fig. 3. For incidence of linearly polarized LG beam with $\ell = 1$, there are four SPP beams (1~4) generated on the metal surface, as shown in Fig. 3a. It should be mentioned that the amplitudes of beams 1 and 4 are stronger than that of beams 2 and 3. According to the wavevector matching condition depicted in Fig. 2, the SPP beams 1~4 are generated with the aid of the in-plane wavevectors $\mathbf{k}_{\text{OAM}} = \mathbf{k}_a \sim \mathbf{k}_d$, respectively. Note that \mathbf{k}_a and \mathbf{k}_c are provided by the left half part of the LG beam spot while \mathbf{k}_b and \mathbf{k}_d by the right. The SPP beam 2 should suffer more propagation loss than beam 1 since the former is initially generated at the left side of the incident beam spot with the aid of \mathbf{k}_c and propagates on the right. The SPP beam 3 is weaker than 4 because it is generated at the right of the incident spot and propagate along the left direction. When the topological charge becomes negative, the in-plane wavevector changes to opposite direction at every point. Thus, we can observe the generated SPP beams 2, 3 are stronger than 1, 4 as shown in

Fig. 3b. The lateral profiles of SPP field amplitudes show the amplitude differences of the four SPP beams, as shown in Fig. 3a and b. The amplitude of beam 1 or 4 is up to 40% larger than that of beam 2 or 3 as $\ell = 1$. The amplitude differences of beam 2, 3 and 1, 4 remain the same value as $\ell = -1$. It should be mentioned that if the horizontal linear polarization is rotated by 90° , the phase difference of \mathbf{E}_1 and \mathbf{E}_2 components changes from π to 0. Neither will destructive interference of SPPs happen on both sides of the MNA. The results for vertical linear polarization are the same with that for horizontal polarization in Fig. 3a and b.

Next, we change the polarization of LG beam to be circular. For LG beam with LCP, the excited SPPs should propagate along the left direction for both $\ell = \pm 1$ and only beams 1, 3 are generated, as shown in Fig. 3c and d. The results coincide with our theoretical analysis. The SPP beam 1 is stronger than 3 for $\ell = 1$ and the result reverses for $\ell = -1$ since they are excited by different parts of the LG beam spot. For LG beam with RCP, the excited SPPs propagate along the right direction and only beams 2, 4 appear. The SPP beam 4 is stronger than 2 for $\ell = 1$ and the beam 2 becomes stronger for $\ell = -1$, as shown in Fig. 3e and f.

According to the wavevector matching condition shown in Fig. 2b, the splitting angle α of excited SPP beams is given by

$$\alpha = 2\text{acos} \left(\frac{|\mathbf{k}_{\text{SPP}}|^2 + |\mathbf{G}|^2 - |\mathbf{k}_{\text{OAM}}|^2}{2|\mathbf{k}_{\text{SPP}}| \cdot |\mathbf{G}|} \right). \quad (5)$$

The splitting angle as a function of the MNA period is depicted in Fig. 4a. We perform FDTD simulations of MNA composed of six columns of nanoapertures with varying periods. The LG beam with RCP and topological charge $\ell = 1$ is illuminated on the MNA. The numerical results agree well with the theoretical predictions. It is found that α increases from 20.02 to 23.92° as the period increases from 0.55 to 0.62 μm . Then, it begins to decrease as p increases. Such a trend can be deduced from the wavevector matching condition. As the period of MNA determines the reciprocal lattice vector \mathbf{G} and the amplitudes of \mathbf{k}_{SPP} and \mathbf{k}_{OAM} are fixed, the maximum of splitting angle appears when \mathbf{k}_{OAM} is vertical to \mathbf{G} . Under this condition, we can predict that the maximum splitting angle locates at $p = 0.62$ μm , which coincides well with the numerical result. In addition, the splitting angle is also tunable by varying the incident wavelength. Note that both the SPP wavevector and in-plane wavevector of LG beam are varying with the incident wavelength as indicated in Eqs. (1) and (3). We perform numerical simulations for incident LG beam with RCP and $\ell = 1$. The period of the MNA is fixed at $p = 0.6$ μm . Figure 4 b shows the analytical and numerical results of the SPP splitting angle for different incident wavelengths. In the range $\lambda = 0.55 \sim 0.65$ μm , α increases from 17.1 to 29.4° . The maximum angle appears when $\lambda = 0.65$ μm . Then, the splitting angle decreases to $\alpha = 27.17^\circ$ at $\lambda = 0.7$ μm , which also agrees well the theoretical analysis.

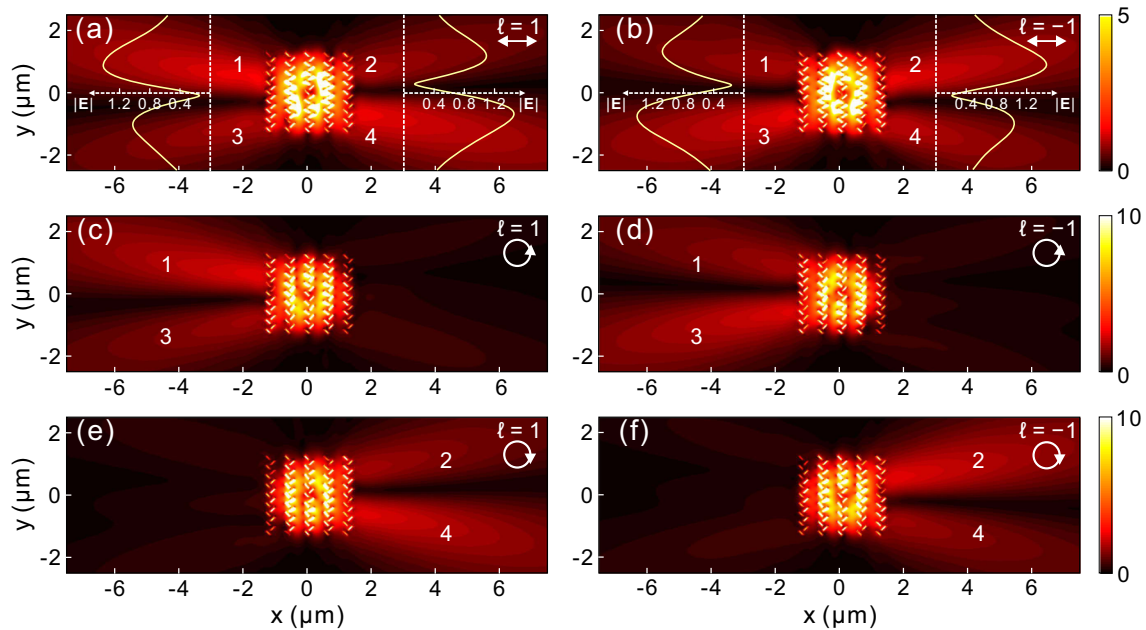


Fig. 3 FDTD simulation results of the electric field distributions ($|E|$) on the metal surface illuminated by LG beams with **a** linear polarization and $\ell = 1$, **b** linear polarization and $\ell = -1$, **c** LCP and $\ell = 1$, **d** LCP and $\ell = -1$

e RCP and $\ell = 1$, **f** RCP and $\ell = -1$. The SPP beams excited in different directions are labeled with the numbers 1~4. The insets in **a** and **b** depict the lateral profiles of SPP field amplitudes

Therefore, by altering the structural period and incident wavelength, the splitting angles of SPP beams could be largely tailored.

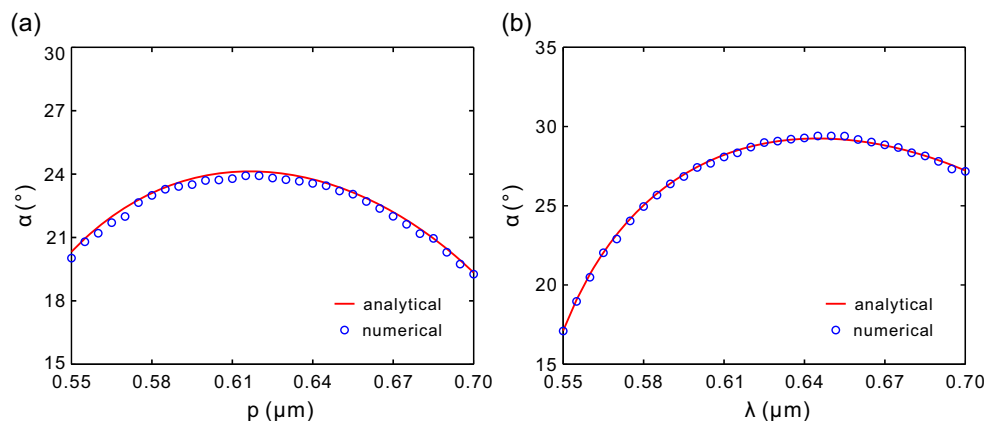
In order to obtain single directional excitation of SPPs, we construct a composite structure with different periods of MNAs. As shown in Fig. 5a, the periods of the two MNAs on the left and right are denoted by p_1 and p_2 , respectively. Then, the corresponding reciprocal lattice vectors are $G_1 = 2\pi/p_1$ and $G_2 = 2\pi/p_2$. As the center of LG vortex beam is aligned to the middle of the structure, the OAM on the left (right) part of LG beam should interact with the left (right) MNA. The wavevector matching conditions are shown in Fig. 5b as $\ell = \pm 1$. For $\ell = 1$, only the in-plane wavevectors \mathbf{k}_a and \mathbf{k}_b take effect in matching Eq. (4). It is apparent that there are $\mathbf{k}_{OAM} = \mathbf{k}_a$ on the left and $\mathbf{k}_{OAM} = \mathbf{k}_b$ on the right. Consequently, the SPPs beams 1 and 4 can be excited. For

$\ell = -1$, we have $\mathbf{k}_{OAM} = \mathbf{k}_c$ on the left and $\mathbf{k}_{OAM} = \mathbf{k}_d$ on the right. The SPPs beams 2 and 3 can be excited. The angles between \mathbf{G} and \mathbf{k}_{OAM} are denoted by θ_1 and θ_2 in the left and right MNA arrays, respectively. For the composite MNAs structure, the angles can be given by

$$\begin{aligned} \theta_1 &= \arccos\left(\frac{|\mathbf{k}_{SPP}|^2 + |\mathbf{G}_1|^2 - |\mathbf{k}_{OAM}|^2}{2|\mathbf{k}_{SPP}| \cdot |\mathbf{G}_1|}\right), \quad \theta_2 \\ &= \arccos\left(\frac{|\mathbf{k}_{SPP}|^2 + |\mathbf{G}_2|^2 - |\mathbf{k}_{OAM}|^2}{2|\mathbf{k}_{SPP}| \cdot |\mathbf{G}_2|}\right). \end{aligned} \quad (6)$$

If the periods of the two MNAs in the composite structure are chosen such that $G_1 + G_2 = 2k_{SPP}\cos\theta$, we can have $\theta = \theta_1 = \theta_2$, which means that the SPP beams propagate in

Fig. 4 Splitting angle α of SPP beams as a function of **a** MNA period p and **b** incident wavelength. The LG beam is with RCP and $\ell = 1$. The red solid curve and blue circles represent the analytical and numerical simulation results, respectively



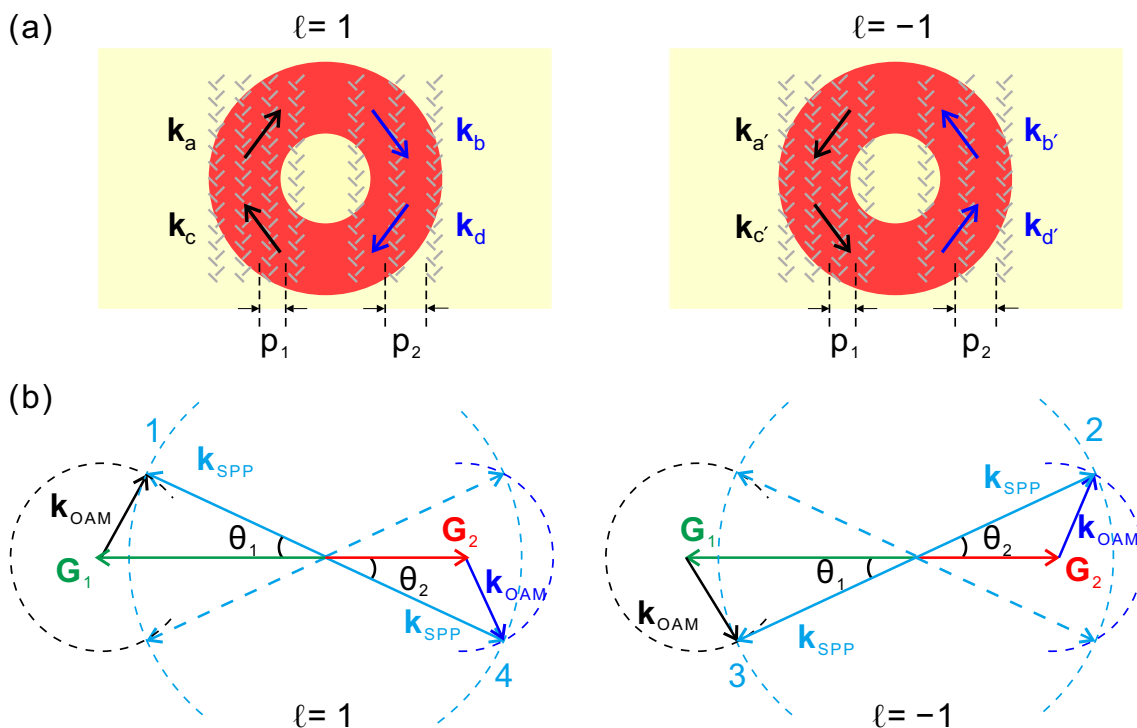


Fig. 5 **a** Structure of composite MNAs and in-plane wavevectors associated with the OAMs of LG beams for $\ell = \pm 1$. The periods of the two MNAs are p_1 and p_2 , respectively. **b** Wavevector matching conditions for $\ell = \pm 1$. \mathbf{G}_1 and \mathbf{G}_2 represent the reciprocal lattice vectors of the two

MNAs. There should be $\mathbf{k}_{\text{OAM}} = \mathbf{k}_a$ or \mathbf{k}_b for $\ell = 1$ and $\mathbf{k}_{\text{OAM}} = \mathbf{k}_{c'}$ or $\mathbf{k}_{d'}$ for $\ell = -1$. θ_1 and θ_2 are azimuthal angles indicating the propagation directions of SPPs. In the implementation, we set $\theta_1 = \theta_2$

opposite directions. Obviously, as the incident LG beams are circularly polarized, SPPs shall propagate along a single direction.

Numerical simulations are performed to verify the above analysis. In the calculation, we have $p_1 = 500$ nm and $p_2 = 778$ nm. The other parameters of the composite MNAs are

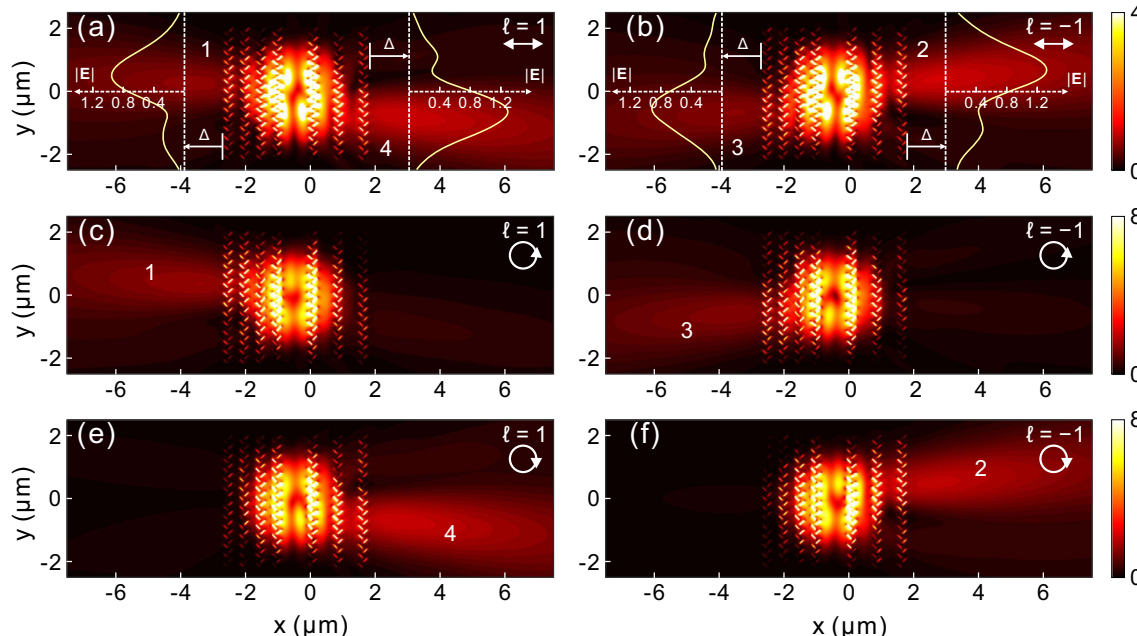


Fig. 6 Electric field distributions of SPPs excited by the composite MNAs under illumination of LG beams with **a** linear polarization and $\ell = 1$, **b** linear polarization and $\ell = -1$, **c** LCP and $\ell = 1$, **d** LCP and $\ell = -$

e RCP and $\ell = 1$, **f** RCP and $\ell = -1$. The insets in **a** and **b** depict the lateral profiles of SPP field amplitudes at a distance of $\Delta = 1.2$ μm from the array boundaries

the same with that of the uniform array. The LG beam is normally incident on the middle of the two MNAs. For linearly polarized LG beam with $\ell = 1$, SPP beams 1 and 4 are respectively excited on the left and right sides, as shown in Fig. 6a. As the topological charge is negative, SPP beams 2 and 3 are launched, as shown in Fig. 6b. The simulation results coincide well with the wavevector matching condition. The insets of Fig. 6a and b show the lateral profiles of SPP amplitudes. The amplitudes are recorded at a distance of $\Delta = 1.2 \mu\text{m}$ from the array boundaries. It is found that the amplitude of beam 4 is $\sim 40\%$ larger than that of beam 1 as $\ell = 1$. The amplitude differences of beam 2 and 3 remain the same value as $\ell = -1$. In Fig. 6c, only SPP beam 1 appears in the left array as the incident LG beam is with LCP and $\ell = 1$. For RCP incidence, only SPP beam 4 is excited in the right direction as presented in Fig. 6e. When $\ell = -1$, the LG beam with LCP is converted to SPP beam 3 and propagates in the left lower direction, as shown in Fig. 6d. While for LG beam with RCP, SPP beam 2 is launched in the right upper direction, as shown in Fig. 6f. The simulated results are $\theta = \theta_1 = \theta_2 = 7.78^\circ$. The results verify that unidirectional SPP beam can be obtained using circularly polarized LG beams impinging on the composite MNA structure. Therefore, we can achieve unidirectional SPPs excitation by manipulating the polarization and the topological charge of the LG beam.

Conclusion

In conclusion, we have investigated the excitation control of SPPs on a metal surface using circularly polarized LG beams. In order to realize the coupling between SPPs and normally incident LG beams, a MNA structure is employed. The side direction of SPP excitation on the metal surface is determined by the circular polarization of the incident beam. As the light with LCP is incident, SPPs are excited and propagate on the left side of the array. On the contrary, SPPs should propagate on the right. As the incident LG beams possess OAM, which is determined by the topological charge, the excited SPPs will experience beam splitting on each side of the array. Furthermore, the composite MNAs with different periods are also utilized to control the SPP excitation direction by manipulating the wavevector matching condition. By varying the topological charge and circular polarization direction of the incident beam, SPPs can be finally generated on either side of the array and propagate along a certain fixed direction. The study may have great applications in developing compact plasmonic devices such as optical switches and SPP generators.

Funding Information This work was supported by the National Natural Science Foundation of China (Grant No. 11674117).

References

- Barnes WL, Dereux A, Ebbesen TW (2003) Surface plasmon sub-wavelength optics. *Nature* 424(6950):824–830
- Zayats AV, Smolyaninov II, Maradudin AA (2005) Nano-optics of surface plasmon polaritons. *Phys Rep* 408(3–4):131–314
- Zayats AV, Smolyaninov II (2003) Near-field photonics: surface plasmon polaritons and localized surface plasmons. *J Opt A Pure Appl Opt* 5(4):S16–S50
- Kauranen M, Zayats AV (2012) Nonlinear plasmonics. *Nat Photonics* 6(11):737–748
- Hu GW, Hong XM, Wang K, Wu J, Xu HX, Zhao WC, Liu WW, Zhang S, Garcia-Vidal F, Wang B, Lu PX, Qiu CW (2019) Coherent steering of nonlinear chiral valley photons with a synthetic Au-WS₂ metasurface. *Nat Photonics* 13(7):467–472
- Chen J, Wang K, Long H, Han X, Hu H, Liu W, Wang B, Lu P (2018) Tungsten disulfide-gold Nanohole hybrid metasurfaces for nonlinear metalenses in the visible region. *Nano Lett* 18(2):1344–1350
- Butet J, Brevet PF, Martin OJ (2015) Optical second harmonic generation in plasmonic nanostructures: from fundamental principles to advanced applications. *ACS Nano* 9(11):10545–10562
- Zhang Y, Grady NK, Ayala-Orozco C, Halas NJ (2011) Three-dimensional nanostructures as highly efficient generators of second harmonic light. *Nano Lett* 11(12):5519–5523
- Zhang HC, Fan Y, Guo J, Fu X, Cui TJ (2015) Second-harmonic generation of spoof surface plasmon polaritons using nonlinear plasmonic metamaterials. *Acs Photonics* 3(1):139–146
- Shao DB, Chen SC (2005) Surface-plasmon-assisted nanoscale photolithography by polarized light. *Appl Phys Lett* 86(25):253107
- Luo X, Ishihara T (2004) Subwavelength photolithography based on surface-plasmon polariton resonance. *Opt Express* 12(14):3055–3065
- Berini P (2014) Surface plasmon photodetectors and their applications. *Laser Photonics Rev* 8(2):197–220
- Yu ZF, Veronis G, Fan SH, Brongersma ML (2006) Design of midinfrared photodetectors enhanced by surface plasmons on grating structures. *Appl Phys Lett* 89(15):151116
- Echtermeyer TJ, Milana S, Sassi U, Eiden A, Wu M, Lidorikis E, Ferrari AC (2016) Surface plasmon polariton graphene photodetectors. *Nano Lett* 16(1):8–20
- Schuller JA, Barnard ES, Cai W, Jun YC, White JS, Brongersma ML (2010) Plasmonics for extreme light concentration and manipulation. *Nat Mater* 9(3):193–204
- Atwater HA, Polman A (2010) Plasmonics for improved photovoltaic devices. *Nat Mater* 9(3):205–213
- Garcia MA (2012) Surface plasmons in metallic nanoparticles: fundamentals and applications. *J Phys D Appl Phys* 45(38):389501
- Shchegrov AV, Novikov IV, Maradudin AA (1997) Scattering of surface plasmon polaritons by a circularly symmetric surface defect. *Phys Rev Lett* 78(22):4269–4272
- Ozbay E (2006) Plasmonics: merging photonics and electronics at nanoscale dimensions. *Science* 311(5758):189–193
- Bar-Lev D, Arie A, Scheuer J, Epstein I (2015) Efficient excitation and control of arbitrary surface plasmon polariton beams using one-dimensional metallic gratings. *Physics J Opt Soc Am B* 32(5):923–932
- Sun ZJ, Jung YS, Kim HK (2003) Role of surface plasmons in the optical interaction in metallic gratings with narrow slits. *Appl Phys Lett* 83(15):3021–3023
- Torosyan G, Rau C, Pradarutti B, Beigang R (2004) Generation and propagation of surface plasmons in periodic metallic structures. *Appl Phys Lett* 85(16):3372–3374
- Sonnefraud Y, Kerman S, Di Martino G, Lei DY, Maier SA (2012) Directional excitation of surface plasmon polaritons via nanoslits

- under varied incidence observed using leakage radiation microscopy. *Opt Express* 20(5):4893–4902
24. Wang B, Aigouy L, Bourhis E, Gierak J, Hugonin JP, Lalanne P (2009) Efficient generation of surface plasmon by single-nanoslit illumination under highly oblique incidence. *Appl Phys Lett* 94(1):011114
 25. Xu T, Zhao YH, Gan DC, Wang CT, Du CL, Luo XG (2008) Directional excitation of surface plasmons with subwavelength slits. *Appl Phys Lett* 92(10):101501
 26. Li XW, Tan QF, Bai BF, Jin GF (2011) Experimental demonstration of tunable directional excitation of surface plasmon polaritons with a subwavelength metallic double slit. *Appl Phys Lett* 98(25):251109
 27. López-Tejiera F, Rodrigo SG, Martín-Moreno L, García-Vidal FJ, Devaux E, Ebbesen TW, Krenn JR, Radko IP, Bozhevolnyi SI, González MU, Weeber JC, Dereux A (2007) Efficient unidirectional nanoslit couplers for surface plasmons. *Nat Phys* 3(5):324–328
 28. Chen J, Li Z, Yue S, Gong Q (2010) Efficient unidirectional generation of surface plasmon polaritons with asymmetric single-nanoslit. *Appl Phys Lett* 97(4):041113
 29. Kim H, Lee B (2009) Unidirectional surface plasmon polariton excitation on single slit with oblique backside illumination. *Plasmonics* 4(2):153–159
 30. Huang X, Brongersma ML (2013) Compact aperiodic metallic groove arrays for unidirectional launching of surface plasmons. *Nano Lett* 13(11):5420–5424
 31. Pors A, Nielsen MG, Bernardin T, Weeber JC, Bozhevolnyi SI (2014) Efficient unidirectional polarization-controlled excitation of surface plasmon polaritons. *Light-Sci Appl* 3(8):e197–e197
 32. Radko IP, Bozhevolnyi SI, Bruccoli G, Martín-Moreno L, García-Vidal FJ, Boltasseva A (2009) Efficient unidirectional ridge excitation of surface plasmons. *Opt Express* 17(9):7228–7232
 33. Baron A, Devaux E, Rodier JC, Hugonin JP, Rousseau E, Genet C, Ebbesen TW, Lalanne P (2011) Compact antenna for efficient and unidirectional launching and decoupling of surface plasmons. *Nano Lett* 11(10):4207–4212
 34. Liu Y, Palomba S, Park Y, Zentgraf T, Yin X, Zhang X (2012) Compact magnetic antennas for directional excitation of surface plasmons. *Nano Lett* 12(9):4853–4858
 35. Yang J, Xiao X, Hu C, Zhang W, Zhou S, Zhang J (2014) Broadband surface plasmon polariton directional coupling via asymmetric optical slot nanoantenna pair. *Nano Lett* 14(2):704–709
 36. Ding F, Deshpande R, Bozhevolnyi SI (2018) Bifunctional gap-plasmon metasurfaces for visible light: polarization-controlled unidirectional surface plasmon excitation and beam steering at normal incidence. *Light-Sci Appl* 7(4):17178
 37. Du L, Kou SS, Balaur E, Cadusch JJ, Roberts A, Abbey B, Yuan XC, Tang D, Lin J (2015) Broadband chirality-coded meta-aperture for photon-spin resolving. *Nat Commun* 6:10051
 38. Lin J, Mueller JP, Wang Q, Yuan G, Antoniou N, Yuan XC, Capasso F (2013) Polarization-controlled tunable directional coupling of surface plasmon polaritons. *Science* 340(6130):331–334
 39. Huang LL, Chen XZ, Bai BF, Tan QF, Jin GF, Zentgraf T, Zhang S (2013) Helicity dependent directional surface plasmon polariton excitation using a metasurface with interfacial phase discontinuity. *Light-Sci Appl* 2(3):e70–e70
 40. O'Connor D, Ginzburg P, Rodríguez-Fortuno FJ, Wurtz GA, Zayats AV (2014) Spin-orbit coupling in surface plasmon scattering by nanostructures. *Nat Commun* 5:5327
 41. Bliokh KY, Rodríguez-Fortuño FJ, Nori F, Zayats AV (2015) Spin-orbit interactions of light. *Nat Photonics* 9(12):796–808
 42. Chen J, Chen X, Li T, Zhu SN (2018) On-chip detection of orbital angular momentum beam by plasmonic nanogratings. *Laser Photonics Rev* 12(8):1700331
 43. Allen L, Beijersbergen MW, Spreeuw RJ, Woerdman JP (1992) Orbital angular momentum of light and the transformation of Laguerre-Gaussian laser modes. *Phys Rev A* 45(11):8185–8189
 44. Yao AM, Padgett MJ (2011) Orbital angular momentum: origins, behavior and applications. *Adv Opt Photonics* 3(2):161–204
 45. Zhan Q (2006) Properties of circularly polarized vortex beams. *Opt Lett* 31(7):867–869
 46. Palik ED (1998) *Handbook of optical constants of solids*, vol 3. Academic press

Publisher's Note Springer Nature remains neutral with regard to jurisdictional claims in published maps and institutional affiliations.